Lasers in Manufacturing Conference 2023

Bimetallic structure formation from powder mixture by laser powder bed fusion

Ada Steponavičiūtė[a,*], Karolis Stravinskas[a], Aušra Selskienė[a], Genrik Mordas[a]

[a]*Center for Physical Sciences and Technology, Vilnius, LT-02300, Lithuania*

Abstract

Bimetallic structures are an excellent solution for a lot of engineering applications which require varying properties at different locations of the same object. Implementation of such structures into engineering fields can lead to easier maintenance, economical and space savings and can also open wider application possibilities. In recent years, production of bimetallic structures has been made possible with help of additive manufacturing (AM) technologies. Using laser powder-bed fusion AM, bimetallic structures can be created by depositing different materials in a layer-by layer fashion. In this work, two materials in powder form were used for bimetallic structure formation – CoCrMo and 17-4 PH stainless-steel. Two different bimetallic structures – one sandwich-like and one made from the two-material powder mixture, were successfully produced by using the L-PBF technology. In-depth analysis of the 17-4 PH and CoCrMo materials and microstructural properties of the produced bimetallic samples were investigated. A gradual change in chemical element distribution is observed at the two-material fusion zone of the sandwich-like specimen while the mixed powder specimen showed even elemental distribution throughout the alloy. The thickness of the fusion zone in the sandwich-like specimen is around 600-630 µm. The hardness values of the fusion zone (46±1 HRC) and of the mixed powder alloy (44±1) are higher than the hardness of 17-4 PH (43±1 HRC) but lower than CoCrMo (50±1 HRC). The experimentally evaluated density of the sandwich-like and mixed powder bimetallic specimens are 7.96 g/cm^3 and 8.06 g/cm^3 respectively. The difference in values proves that the bimetallic alloy possesses unique characteristics that are not specific to either of the materials.

Keywords: additive manufacturing; laser powder bed fusion; bimetallic structure

1. Introduction

Additive manufacturing (AM) is an increasingly popular field of engineering that has attracted significant attention in both academia and industry in recent years. Compared to traditional manufacturing methods, AM

* Corresponding author. Tel.: +370 5 266 1640;
E-mail address: ada.steponaviciute@ftmc.lt

offers numerous advantages including high production efficiency, design freedom, flexibility, and exceptional part performance (Gibson et al, 2014; Parker, 2016). Among the various AM technologies, laser powder bed fusion (L-PBF) is widely used and employs a laser beam to melt powder particles, enabling the production of metal parts. The L-PBF process boasts a rapid cooling rate ranging from 103-108 K/s, leading to refined grains and improved alloy properties due to enhanced nucleation rates (Chen at al., 2017; Bai et al., 2017). As a result, L-PBF finds widespread application in manufacturing metal parts using a wide range of materials such as 316L and 17-4 PH stainless steel, maraging steel, aluminum, titanium, copper, and CoCrMo alloys (Bai et al., 2020). Numerous research papers delve into the microstructure and mechanical properties of these alloys and the influence of heat treatment and manufacturing process conditions on these properties.

However, a limited amount of research papers discusses the production of multi-material parts using L-PBF. It is recognized that integrating multiple materials can lead to tailored chemical and mechanical properties in the manufactured parts, including electrical and thermal conductivity, hardness, corrosion resistance, and more (Chen et al., 2020). Bimetallic structures, in comparison to single-material structures, can offer solutions to a range of engineering challenges and add value to the final product.

Several techniques can be employed to fabricate a bimetallic structure utilizing L-PBF. These approaches include printing one material onto a conventionally manufactured substrate composed of a different material (Shakerin et al., 2019), sequentially printing one material after another (Sing et al., 2015) or combining two powders within a single layer through mixing (Wei et al., 2018).

This research aims to examine a bimetallic structure produced through L-PBF, which comprises 17-4 PH stainless steel and CoCrMo alloy. The combination of these materials aims to enhance the hardness and corrosion resistance of the alloy while preserving the magnetic properties inherent to 17-4 PH stainless steel. Two different types of bimetallic specimens (one with a sandwich-like configuration and one from a powder mixture) are fabricated and analyzed. The morphology, distribution of elements and hardness of both specimens are thoroughly investigated.

2. Experiments

2.1. Material characterization

Table 1. Chemical composition (wt. %) of CoCrMo and 17-4 PH stainless-steel (EOS, Carpenter Additive).

Element	CoCrMo	17-4 PH
Fe	≤0.75	balance
Co	balance	-
Cr	25.0-30.0	15.0-17.0
Ni	≤0.1	3.0-5.0
Mo	5.0-7.0	<1.0
C	≤0.16	<0.1
Mn	≤1.0	<1.0
Si	≤1.0	<1.0
Cu	-	3.0-5.0
Nb+Ta	-	0.2-0.5

For the experiment, two different metal powders were selected: 17-4 PH stainless steel from Carpenter Additive and MP1 CoCrMo powder from EOS. The chemical composition of both materials can be found in

Table 1. Scanning electron microscopy (SEM) was employed to examine the particle morphology of these powders. The experiment utilized a Helios NanoLab 650 SEM equipped with an energy dispersion X-ray spectrometer (INCAEnergy). The SEM system features a Schottky-type field emission electron source and a focused Ga ion source. Element mappings were conducted with an accelerating voltage of 20 kV and a beam current of 1.6 nA. The powder particles were deposited onto a carbon film and subsequently subjected to analysis.

2.2. Sample preparation

The experiments were conducted in N_2 gas atmosphere using an EOSINT M280 L-PBF machine from EOS. The machine is equipped with a 200 W 1060 nm IPG built-in Yb fibre laser and a high-speed scanner featuring a precision galvanometer (11 µrad) with temperature compensation. The process parameters remained consistent for both materials in the sandwich-like specimen and for the mixed powder specimen. These parameters included a laser power of 163 W, scanning speed of 670 mm/s, hatching distance of 0.1 mm, and layer thickness of 40 µm. A scanning strategy involving 4 mm stripes with a rotation angle of 67 degrees after each layer was employed for both materials. These specific process parameters ensured a volumetric energy density value that led to high relative density in both alloys, primarily due to their similar melting temperatures.

For the sandwich-like specimen, a CoCrMo part (20 x 20 x 5 mm) was built on a stainless-steel build platform heated to 80 °C with a 3 mm support structure and then a 17-4 PH stainless-steel structure of the same dimensions was built on top of the CoCrMo part. Switching between the different powders was manually performed by pausing the printing process and replacing the CoCrMo powder with 17-4 PH stainless steel powder in the machine. The printing process was only resumed once the oxygen concentration in the build chamber reached 0.7%. Any potential negative impact on the bonding of the two materials resulting from the temperature drop during the material change will be further investigated in this study.

For the mixed powder sample, CoCrMo and 17-4 PH powders were mixed with a 1:1 ratio before printing. A 20 x 20 x 10 mm sample was built on a stainless-steel build platform heated to 80 °C with a 3 mm support structure.

2.3. Sample characterization

A cross-sectional slice of the specimen was made, and the microstructure was examined using the same scanning electron microscopy (SEM). During the SEM observations, energy dispersive spectroscopy (EDS) was utilized to conduct analysis and mapping of element distribution.

Density measurements were carried out using the Radwag AS 520.R2 PLUS analytical balance. To determine density, the sample was first weighed in air and then weighed again in water. By measuring the known temperature of the water and entering it into the analytical balance, the density determination was automatically displayed on the balance's screen.

For hardness evaluation, a THBRV-187.5D hardness tester in the Rockwell scale was used, employing a spheroconical diamond indenter with a load of 150 kg and a dwell time of 5 seconds. For the sandwich-like specimen, measurements were performed on the cross-sectional surface in three different sections, with each section being measured three times. The sections included the CoCrMo side of the specimen, the 17-4 PH side, and the middle (fusion zone). For the mixed powder specimen, measurements were performed in three different locations on the cross-sectional surface.

3. Results and discussion

3.1. Powder morphology

Figure 1 displays high-resolution images depicting the collection of CoCrMo and 17-4 PH powder metal particles. The images reveal that both powders exhibit a polydisperse distribution of particle sizes ranging from 5 to 50 µm. The size of the largest particles is influenced by the diameter of the atomizer jet nozzle utilized during the production of metal powder (Dunkley, 2015). It is worth mentioning that most of the particles appear spherical in shape, while non-spherical particles are observed as a result of smaller spherical particles adhering and sticking to larger spherical particles.

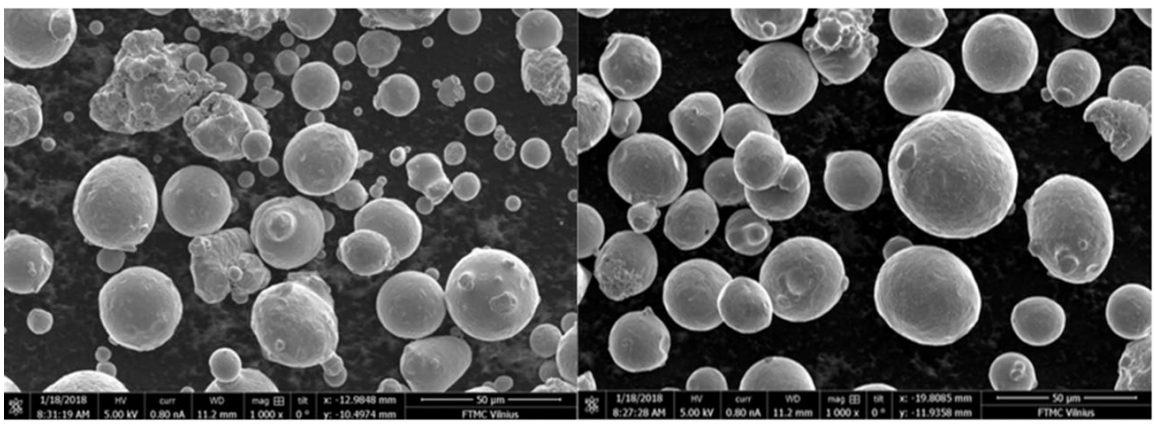

Fig. 1. Particle morphology of the CoCrMo (left) and 17-4 PH (right) powder (scale 50 µm)

3.2. Alloy microstructure and chemical distribution of the sandwich-like specimen

The image in Figure 2 depicts a scanning electron microscope (SEM) micrograph of the fusion zone between 17-4 PH and CoCrMo.

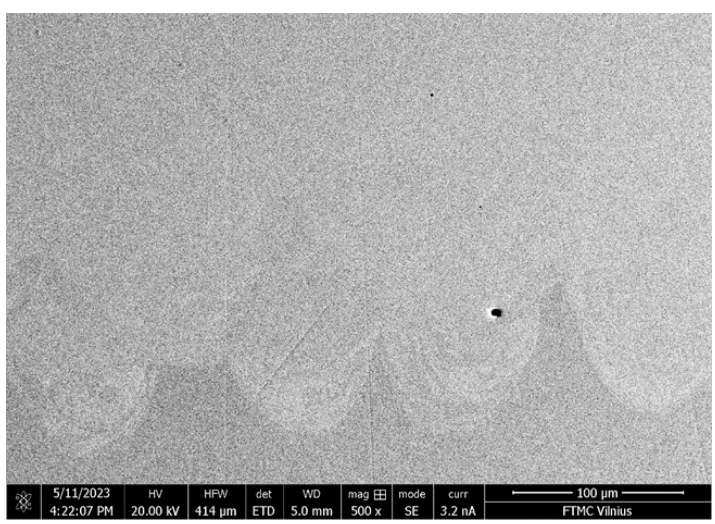

Fig. 2. SEM micrograph of the 17-4 PH/CoCrMo fusion zone

The picture displays distinct shades, with 17-4 PH appearing darker and CoCrMo appearing lighter. There is one distinct pore on the CoCrMo part of the sample, however, there are no visible cracks within the fusion zone, indicating that the two materials exhibit good metallurgical bonding properties.
Additionally, the temperature decrease during the material transition process did not adversely affect the bonding between the two alloys.

The chemical element distribution (wt. %) of the fusion zone is shown in Fig. 3. The red line shows the location of 20 measurements. The start of the fusion zone is indicated by a vertical blue dashed line. On the left side of the line is CoCrMo, while the wavy blue dashed line marks the boundary between the fusion zone and the start of 17-4 PH on the right side. The distribution of elements in the fusion zone is not uniform. Initially (at measurement points 4 to 8), the changes in elemental composition are minimal, with the alloy primarily consisting of CoCrMo and a very low concentration of 17-4 PH. The most significant changes in element distribution occur between measurement points 10 and 18. According to Figure 3, the concentration of Co decreases from 62.01% at point 10 to 35.87% at point 17 and 0% at point 18, while the Fe concentration increases from 1.48% to 78.85%. Changes in the concentration of Cr and Mo can also be observed, although they are less pronounced due to the relatively similar concentration of these elements in both materials.

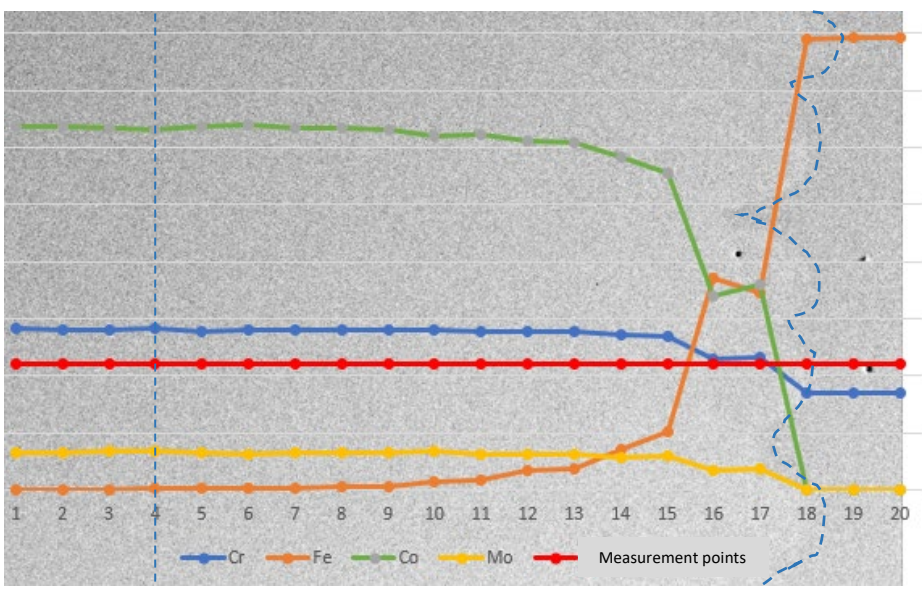

Fig. 3. Chemical element (Cr, Fe, Co, Mo) distribution in the 17-4 PH/CoCrMo fusion zone (red line marks the measurement location)

Despite the uneven elemental distribution in the fusion zone and the minor changes in chemical composition at the beginning of the zone, it was possible to determine the thickness of the fusion zone between the two materials by examining the distribution of chemical elements. The thickness of the fusion zone is around 600-630 µm.

The edge between the fusion zone and the CoCrMo part of the sample was further investigated, and SEM-EDS mapping was carried out to evaluate the chemical element distribution. Figure 4 displays SEM-EDS maps

depicting the distribution of Fe, Co, Cr, and Mo. It can be observed from the maps that the transition between the two materials is non-uniform and is influenced by the depth and position of the melt-pools.

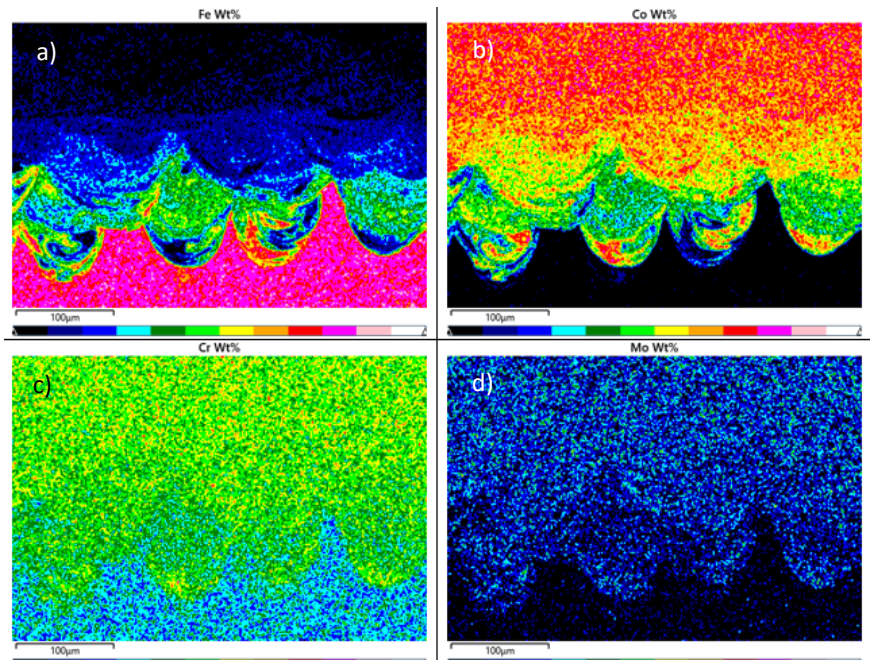

Fig. 4. SEM-EDS maps showing a) Fe, b) Co, c) Cr and d) Mo elemental distribution, %.

3.3. Alloy microstructure and chemical distribution of the mixed powder specimen

The image on the left-hand side in Figure 5 depicts a SEM micrograph of the bimetallic 17-4 PH/CoCrMo specimen printed from powder mixture. The SEM-EDS images in the middle and on the right-hand side show Co and Fe elemental distribution (wt. %) respectively. It can be seen from the images that the elemental distribution is mostly even with only some parts of the micrograph showing differences in concentration. The reason for the uneven elemental distribution might be not sufficient mixing of the two powders during material preparation. Chemical composition of the bimetallic alloy is provided in Table 2.

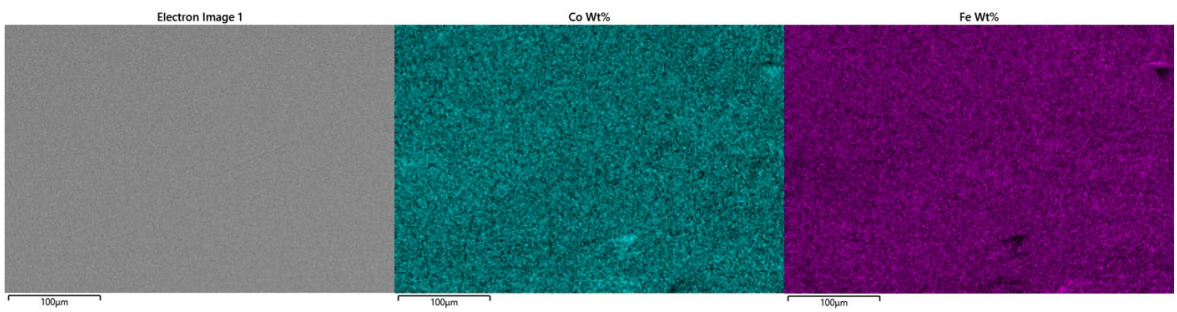

Fig. 5. SEM micrograph of the 17-4 PH/CoCrMo mixed powder specimen (left), Co elemental distribution (wt. %) (middle) and Fe elemental distribution (wt. %) (right)

Table 2. Chemical composition of the 17-4 PH/CoCrMo mixed powder specimen

Element	Si	Cr	Mn	Fe	Co	Ni	Cu	Mo
Concentration, wt. %	0.76	22.58	0.58	34.99	34.12	2.05	1.45	3.47

3.4. Hardness and density

For the sandwich-like specimen, hardness was measured in three locations of the sample – 17-4 PH side, CoCrMo side and the fusion zone. Experimental results are listed in Table 3. The hardness of the fusion zone is higher than the hardness of 17-4 PH but lower than CoCrMo. For the specimen printed from 17-4 PH/CoCrMo powder mixture, hardness measurements were performed in various locations of the cross-sectional face of the specimen. The hardness value is slightly lower than the hardness of the fusion zone. This value might be the result of the indenter possibly not being positioned exactly in the fusion zone and more to the CoCrMo side of the sample.

Table 3. Hardness and density of 17-4 PH, CoCrMo, the fusion zone and the mixed powder alloy

Material / position	Hardness, HRC	Density, g/cm^3
17-4 PH	43±1	7.75
CoCrMo	50±1	8.30
Fusion zone	46±1	7.96
Mixed powder alloy	44±1	8.06

According to the material datasheets provided by the powder manufacturers, the density of parts built from 17-4 PH and CoCrMo is 7.75 g/cm^3 and 8.30 g/cm^3 respectively (EOS, Carpenter Additive). The experimentally evaluated density of the bimetallic sandwich-like specimen is 7.96 g/cm^3., mixed powder alloy – 8.06 g/cm^3.

The difference in values proves that both the fusion zone of the sandwich-like specimen and the mixed powder 1-74 PH/CoCrMo alloy possess unique characteristics that are not specific to either of the materials.

4. Conclusions

In this work, two bimetallic CoCrMo and 17-4 PH stainless-steel structures were manufactured by using the L-PBF technology and the characterisation of both materials, the two-material fusion zone and the mixed powder alloy is presented.

1. Both CoCrMo and 17-4 PH stainless-steel powders have a polydisperse particle size distribution from 5 to 50 µm. Particles are spherical, some non-spherical particles are visible, which are caused by smaller spherical particles being attached to larger ones.

2. The changes in elemental distribution in the two-material fusion zone of the sandwich-like specimen are uneven. A gradual change in chemical element distribution is observed. SEM-EDS results have shown that the concentration of Co starts decreasing and drops from 62.01% to 0%, Co concentration

increases from 1.48% to 78.85%. The concentration of Cr and Mo is observed but is not as apparent due to their concentration being similar in both materials.

3. By investigating the chemical element distribution, the thickness of the two-material fusion zone of the sandwich-like specimen was evaluated and is around 600-630 µm.

4. SEM-EDS mapping showed that the mixed powder specimen had an even chemical element distribution throughout the whole alloy.

5. The hardness values of the sandwich-like specimen's fusion zone (46±1 HRC) and of the mixed powder specimen (44±1 HRC) are higher than the hardness of 17-4 PH (43±1 HRC) but lower than CoCrMo (50±2 HRC). The experimentally evaluated density of the bimetallic sandwich-like and mixed powder specimens is 7.96 g/cm^3 and 8.06 g/cm^3 respectively.

References

Bai Y, Yang Y, Wang D, Zhang M. Influence mechanism of parameters process and mechanical properties evolution mechanism of maraging steel 300 by selective laser melting. Mater. Sci. Eng. A 2017;703 p. 116-123.

Bai Y, Zhang J, Zhao C, Li C, Wang H. Dual interfacial characterization and property in multi-material selective laser melting of 316L stainless steel and C52400 copper alloy. Mater. Charact. 2020;167.

Chen J, Yang Y, Song C, Wang D, Wu S, Zhang M. Influence mechanism of process parameters on the interfacial characterization of selective laser melting 316L/CuSn10. Mater. Sci. Eng. A 2020;792.

Chen B, Moon S.K, Yao X, Bi G, Shen J, Umeda J, Kondoh K. Strength and strain hardening of a selective laser melted AlSi10Mg alloy. Scr. Mater. 2017;141 p. 45-49.

Dunkley, J. J. ASM Handbook Powder Metalurgy; Samal, P., Newkirk, J., Eds.; ASM International, 2015; Vol. 7.

Gibson I, Rosen D, Stucker B. Additive Manufacturing Technologies. Sringer New York, New York, NY, 2014.

LPW 17-4 PH specifications: https://carpenteradditive.com/wpcontent/uploads/2016/11/LPW-Powders-Brochure-2017.pdf

Material data sheet: http://ip-saas-eos cms.s3.amazonaws.com/public/4b839242298b3d77/721463526ca053889c9784ec989f3c88/EOS_CobaltChrome_MP1_en.pdf

Parker K.K, Additive manufacturing of metals. Acta Mater 2016;117 p. 371–392.

Shakerin S, Hadadzadeh A, Amirkhiz B.S, Shamsdini S, Li J, Mohammadi M. Additive manufacturing of maraging steel-H13 bimetals using laser powder bed fusion technique, Addit. Manuf. 2019;29.

Sing S.L, Lam L.P, Zhang D.Q, Liu Z.H, Chua C.K. Interfacial characterization of SLM parts in multi-material processing: intermetallic phase formation between AlSi10Mg and C18400 copper alloy, Mater. Charact. 2015;107, p. 220–227.

Wei C, Li L, Zhang X, Chueh Y.H. 3D printing of multiple metallic materials via modified selective laser melting, CIRP Ann. 2018; 67, p. 245–248.